Modelling compressive cracking in concrete by a modified lattice model

M.M. Abreu & J.V. Lemos
Laboratório Nacional de Engenharia Civil, Portugal

J. Carmeliet
Laboratory of Building Physics, Catholic University of Leuven, Belgium

E. Schlangen
Microlab, Fac. Civil Engineering, Delft University of Technology, The Netherlands

ABSTRACT: The article describes recent advances achieved within the Delft lattice model to improve its ability to simulate compressive cracking in brittle or quasi-brittle materials, like plain concrete. The main modification made to the conventional formulation of the beam lattice is the introduction of an extra step when the beams stiffness is removed. When the failure criterion for an element is first attained, the bending and shear stiffnesses are removed, and later the remaining axial stiffness is removed when the same beam fails again. Although the number of calculations needed increase, the model maintains its simplicity. The presented results are promising, as the model is now able to better localize the damage, giving more realistic crack patterns, load/deformation and rigidity-decay curves.

1 INTRODUCTION

In the Delft lattice model the continuum is simulated by a mesh of small one-dimensional elements with adequate stiffness properties (Schlangen & Garboczi 1996, 1997). The linear elastic properties and failure criterion of these elements are adjusted accordingly to the properties of the macroscopic material. At each calculation step, a linear analysis is performed and the rigidity of one element is removed when a failure criterion is attained, in this way simulating the cracking process. The Delft lattice model is therefore often classified as a "repeated linear analysis" type of model. The dimension of the elements may be so small, in relation with the size of the model (10^{-2} to 10^{-4} times smaller), that materials, such as concrete, are at these scales not anymore considered as homogeneous, but as being composed of individual constituents (aggregates, mortar).

In the article, an alternative method consisting in removing the element stiffness stepwise will be presented. First the bending and shear stiffnesses are removed and only if that same element fails again, the remaining axial stiffness will also be removed. The main concept is to reproduce the type of failure behaviour observed for most types of frame structures, in which the frame elements will first loose the ability of transmit moments, while still maintaining the capacity of transmitting axial forces, therefore, inducing a redistribution of the load. The main objective is to improve the lattice ability to simulate less brittle behaviour, especially when subjected to compression forces.

2 MODEL GENERAL DESCRIPTION

The geometry of the lattice model results from the distortion of a regular mesh consisting of equilateral triangles. The amount of distortion is controlled by the variable z as defined by Lilliu & van Mier (2000), where $0 \leq z \leq 1$. If z = 0 is used, a regular mesh is obtained and if z = 1, the maximum distorted mesh is generated (Fig. 1). All the models presented in this article use a value z = 0.9. A quite distorted mesh was preferred in order to make the model fairly independent of the load direction and to introduce some degree of disorder, even when a homogeneous material is modelled.
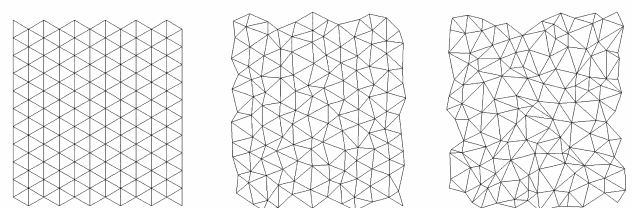
Figure 1 – Lattice mesh examples for z = 0 (left), z = 0.5 (center) and z = 0.9 (right).

A cube of 0.1 × 0.1 × 0.1 m is simulated using a 2-D model. The average beam length ($l_{b,av}$) was set to 2.0 mm. Note that because of the mesh distortion, the true length of a beam (L) will vary. Using this $l_{b,av}$ the lattice model will consist of approximately 8730 beams. The ratio between $l_{b,av}$ and the dimension of the lattice model, will influence the material behaviour. The smaller the beams are the more brittle the material will react. However, for practical reasons, the length $l_{b,av}$ may be limited due to computational restrictions. The length $l_{b,av}$ also depends on the size of small material heterogeneities that we may still want to incorporate (as in the concrete composite model, where the size of the aggregates determines the choice $l_{b,av}$, see section 5).

Besides the difference in length, all beams have identical properties. The beams thickness is 0.1 m to account for the 3D to 2D simplification. The beam height is chosen equal to $0.54 \times l_{b,av}$, which was found to better approximate the target Poisson ratio of 0.2. The elastic modulus of the beam (E) was set equal to 33.9 GPa, in order to approximate the macroscopic elastic modulus of 25.0 GPa.

After selecting the geometry and elastic properties of the beams, the failure condition of the beams has to be chosen. A failure condition similar to the one described by Schlangen & Garboczi (1996), i.e. a tensile limiting failure stress (σ_{lim}), is used. The beam will fail, when the maximum stress in a beam section exceeds this limit. To calculate the stress in a beam a comparative stress (σ_{comp}) is used, instead of the actual elastic stress. This comparative stress σ_{comp} is determined by summing up the stress resulting from the beam axial force and partially the stress resulting from the moment, see Equation 1:

$$\sigma_{comp} = \frac{F}{A} + \alpha \frac{M}{W} \qquad (1)$$

where σ_{comp} = comparative stress; F = axial force; A = beam cross-sectional area; α = weight coefficient; M = bending moment and W = flexure modulus.

The stress resulting from the shear is neglected. The part of the stress resulting from the moment is governed by the variable α, were $0 \leq \alpha \leq 1$. If $\alpha = 0$ the stress resulting from the moments is neglected and if $\alpha = 1$, the stress is fully considered. Note that if $\alpha = 0$, the beams with a negative (compression) axial force will never be able to break, regardless of how high the moment may be. This α-variable determines the brittleness of the model response: a high α results in a more brittle response. In this study $\alpha = 1.0$, 0.5 and 0.0 will be used. The stress σ_{lim} (local tensile strength) is chosen equal to 24.2 MPa, which will result in a material maximum compression stress of 40 MPa for a modified lattice model with $\alpha = 0.5$.

a)   b)
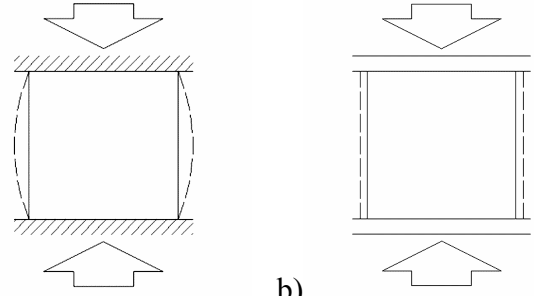
Figure 2 – Boundary conditions: a) "restrained"; b) "unrestrained".

Finally the boundary conditions are generally taken free for the lateral sides of the model. Horizontal and vertical displacements are set equal to zero (restrained conditions) for the bottom and upper sides of the model(Fig. 2a). Although in some analyses all the horizontal displacements were unrestrained (Fig. 2b), these models will be labelled as "unrestrained". The upper side of the model is subjected to a progressive negative displacement in vertical direction resulting in an increasing compressive loading.

3 CONVENTIONAL LATTICE

In a conventional lattice model the rigidity of one beam is removed in one single calculation step. Using this standard formulation, the modelling of cracking in compressive loading becomes problematic, as will be shown by the next examples.

If $\alpha = 0.0$ the model is completely unable to simulate failure as the damage will never localize. Most beams perpendicular to the load direction will sustain tensile loading and thus break (Fig. 3), but the other beams parallel to the load are almost "unbreakable" and will indefinitely continue to transmit the load. The resulting overall loss of the model stiffness is therefore quite low and shows a tendency to stabilization of the stiffness (Fig. 4).
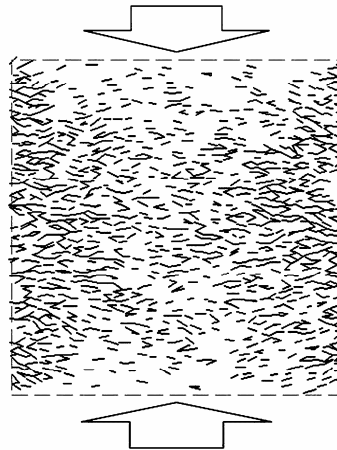
Figure 3 – Beams broken for the conventional model using an $\alpha = 0.0$. The specimen is loaded in compression to a strain of 9 mm/m.
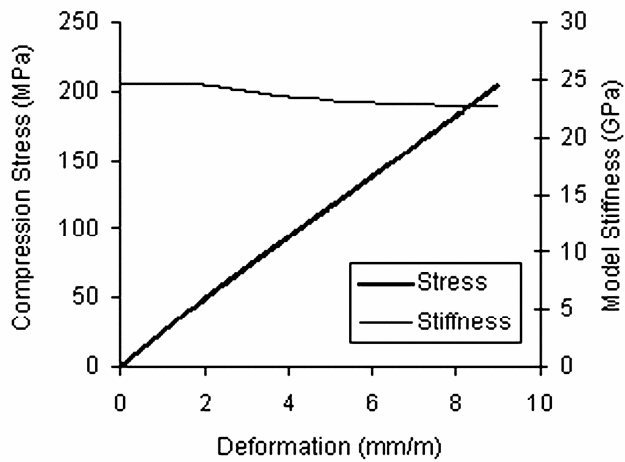
Figure 4 – Stress-strain and stiffness-strain curve for the conventional model with α = 0.0.

In the other extreme case, when α = 1.0, the specimen will break, but in a quite unrealistic way: a main crack is formed, but it crosses through the model from one to the other side. (Fig. 5). The model will behave in a quite brittle way, with an abrupt loss of stiffness and ability to transfer loads (Fig. 6).
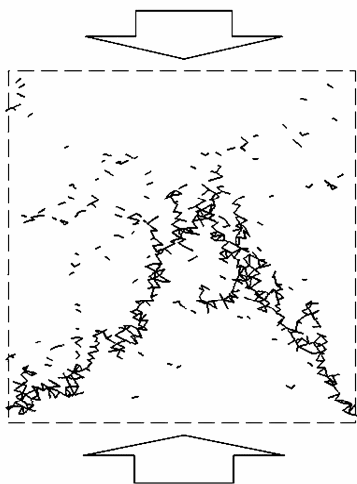
Figure 5 – Beams broken for the conventional model using an α = 1.0 (compressive strain = 0.6 mm/m).
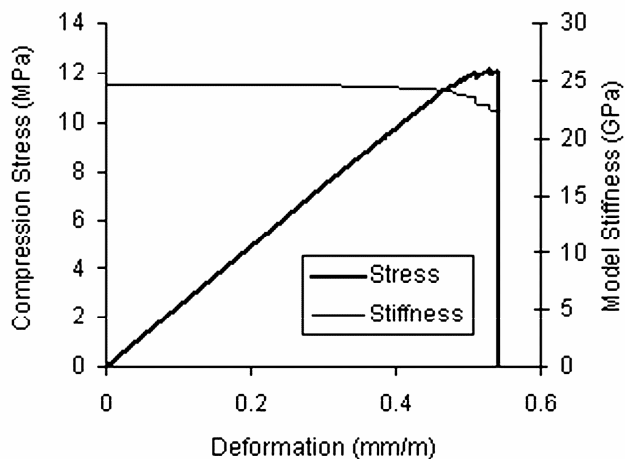
Figure 6 – Stress-strain and stiffness-strain curve for the conventional model with α = 1.0.

If an intermediate value of α=0.5 is used, we still see a quite unrealistic behaviour of the cracking from one to the other side. Now also secondary cracks form, although, they do not link the upper and the bottom part of the model (Fig. 7). The stress--deformation behaviour is still too brittle but the model retains some ability to transfer small loads and so some stiffness remains after main failure (Fig. 8).

Note that not all the calculation steps are presented in the stress-strain and stiffness-strain curves. Only the calculation-steps where an increase on the deformation is observed are presented (in order to maintain the curves simplicity, the backward steps, characteristics of a lattice model, where omitted).
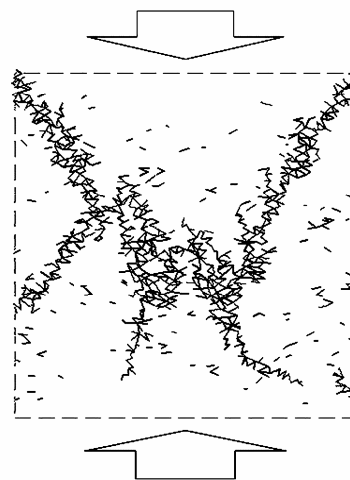
Figure 7 – Beams broken for the conventional model using an α = 0.5 (compressive strain = 1.4 mm/m).
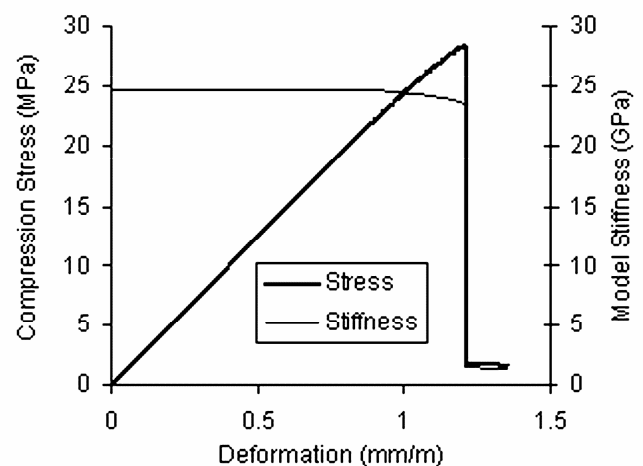
Figure 8 – Stress-strain and stiffness-strain curve for curves for the conventional model with α = 0.5.

4 MODIFIED LATTICE

In the modified lattice model the beam stiffness is removed in two steps: first the bending and shear stiffnesses are removed and only when it fails again in a subsequent calculation (using the same failure criterion) the remaining axial stiffness is removed. So, in the second step the beam element is replaced with a spring element. This is achieved by assigning a beam inertia (I) equal to 0, or a very small value. In the bellow equations 2 and 3, the stiffness matrix of a single element in the first (K^e_1) and second (K^e_2) steps are presented.
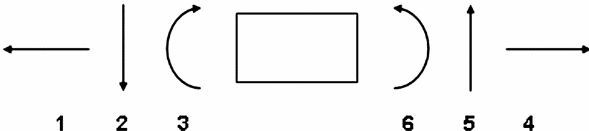
$$K^e_1 = \begin{bmatrix} \dfrac{EA}{L} & 0 & 0 & -\dfrac{EA}{L} & 0 & 0 \\ 0 & \dfrac{12EI}{L^3} & \dfrac{6EI}{L^2} & 0 & -\dfrac{12EI}{L^3} & \dfrac{6EI}{L^2} \\ 0 & \dfrac{6EI}{L^2} & \dfrac{4EI}{L} & 0 & -\dfrac{6EI}{L^2} & \dfrac{2EI}{L} \\ -\dfrac{EA}{L} & 0 & 0 & \dfrac{EA}{L} & 0 & 0 \\ 0 & -\dfrac{12EI}{L^3} & -\dfrac{6EI}{L^2} & 0 & \dfrac{12EI}{L^3} & -\dfrac{6EI}{L^2} \\ 0 & \dfrac{6EI}{L^2} & \dfrac{2EI}{L} & 0 & -\dfrac{6EI}{L^2} & \dfrac{4EI}{L} \end{bmatrix} \quad (2)$$

$$K^e_2 = \begin{bmatrix} \dfrac{EA}{L} & 0 & 0 & -\dfrac{EA}{L} & 0 & 0 \\ 0 & 0 & 0 & 0 & 0 & 0 \\ 0 & 0 & 0 & 0 & 0 & 0 \\ -\dfrac{EA}{L} & 0 & 0 & \dfrac{EA}{L} & 0 & 0 \\ 0 & 0 & 0 & 0 & 0 & 0 \\ 0 & 0 & 0 & 0 & 0 & 0 \end{bmatrix} \quad (3)$$

where K^e_1 = element stiffness matrix in the first step; K^e_2 = element stiffness matrix in the second step; E = elastic modulus of the beam; A = beam cross-sectional area; I = beam moment of inertia; L = beam length.

If α = 0.0 the modified lattice behaves exactly like the conventional lattice mode, and similar results as in figures 3 and 4 are obtained.

If α = 1.0 the compression will originate "X" shaped cracks (Fig. 9). As also represented in the Figure 9, this "X" is formed in 2 phases: first a ">" shaped crack is formed in left part and after an additional "<" shaped crack is formed in the right part of the specimen. Each of these phases corresponds to a noticeable drop on the model stiffness as observed in figure 10. Note also that the model stiffness will now start to decreases already in the pre-peak curve and not just before the peak stress.

If an intermediate α value of 0.5 is chosen, a more realistic cracking behaviour is observed (Figures 11-14). First one part of the specimen starts to detach, then the other part and finally extensive cracking in the centre of the model results in a final rupture of the specimen. Each of these 3 main phases are clearly noticeable in the stress-strain and stiffness-strain curves, corresponding to 3 main drops of the model stiffness. As planned the initial model stiffness is 25 GPa and the peak compression stress is 40 MPa. The peak stress occurs for an imposed deformation of 1.8 mm/m. The model stiffness starts to slightly decay at 0.9 mm/m.
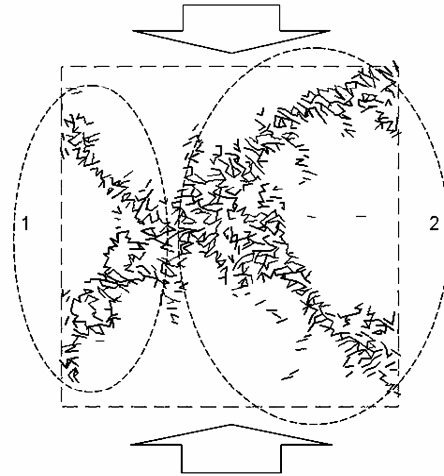
Figure 9 – Beams broken for the modified model using an α = 1.0 (compressive strain = 1.5 mm/m).
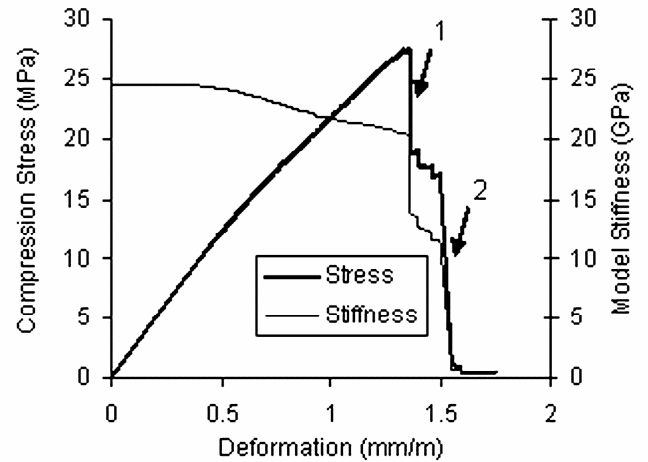
Figure 10 – Stress-strain and stiffness-strain curve for the modified model with α = 1.0.
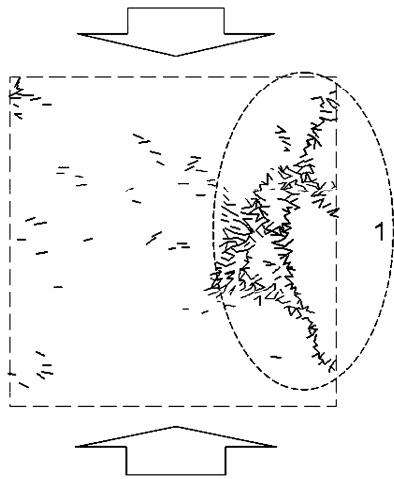
Figure 11 – Beams broken for the modified model using an α = 0.5 (compressive strain = 1.9 mm/m).
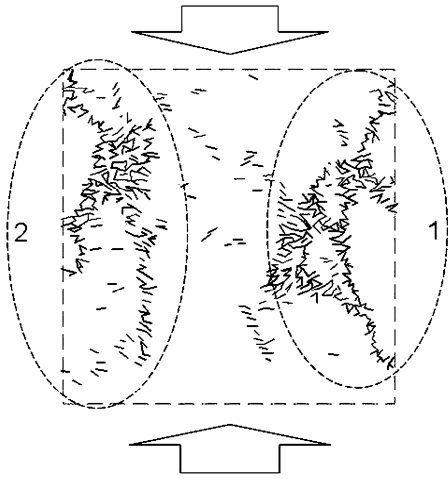
Figure 12 – Same model presented in the figure 11 but for a compressive strain of 2.1 mm/m.
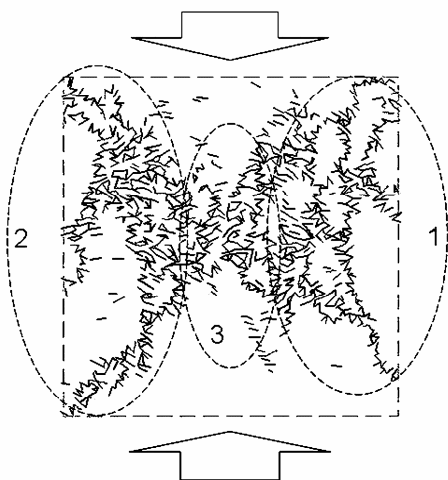
Figure 13 – Same model presented in the figure 11 but for a compressive strain of 3.0 mm/m.
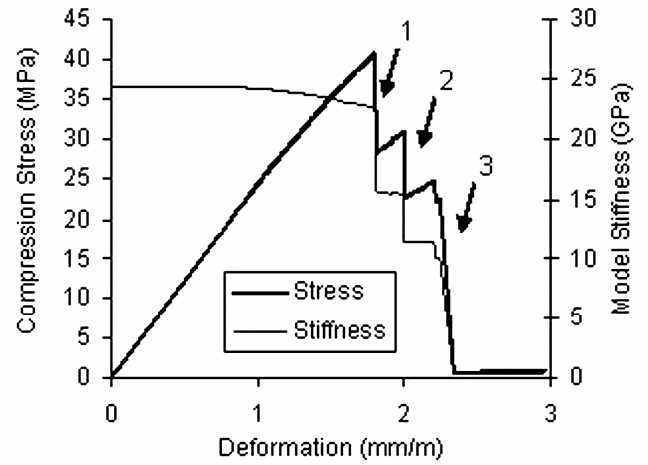
Figure 14 – Stress-strain and stiffness-strain curve for the modified model with α = 0.5.

Until now for all the models the horizontal deformations were restrained at the top and bottom side, where the load is applied, which introduces a high friction between sample and loading plates. In the following example (Figs. 15-16) the horizontal restrains were released (boundary conditions of Figure 2b). As shown in figure 15, the main cracks are now more oblique to the model top and bottom sides. Secondary vertical cracks may also be observed. At this development phase the model cannot simulate completely vertical cracks, like the ones that may be observed for some materials when subjected to these boundary conditions. The initial modulus of elasticity and the peak compression stress are approximately the same, but the model behaviour is now more brittle as shown by the abrupt loss of stiffness in Figure 16.
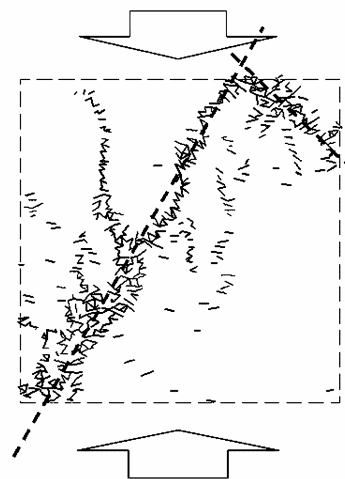
Figure 15 — Beams broken for the modified "unrestrained" model using an α = 0.5 (compressive strain = 2.0 mm/m).
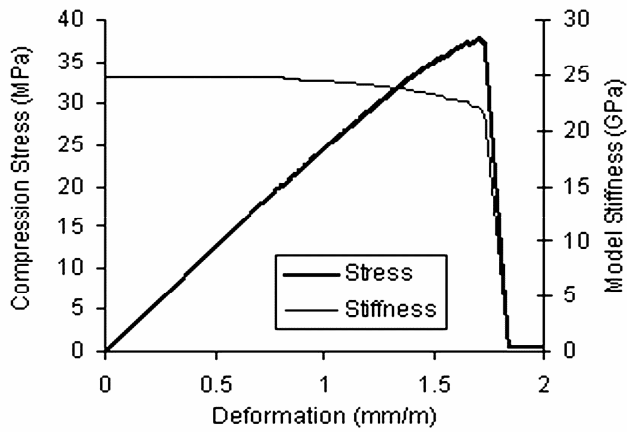
Figure 16 – Stress-strain and stiffness-strain curve for the modified "unrestrained" model with α = 0.5.

5   CONCRETE COMPOSITE MODEL

The next examples illustrate the ability of the lattice model to simulate the damage behaviour of concrete considered as a composite material consisting of mortar and aggregates. Aggregates are conceptually simulated in 2D as circles of two sizes. Real images of concrete cross sections can also be used. This image is then scanned by the model "pixel by pixel". If the starting and ending point of a beam is found inside an aggregate, the beam is marked as "aggregate". The same procedure applies for the mortar. Beams with one point inside an aggregate and the other inside mortar are marked as belonging to the interfacial zone. The resulting model is labelled "concrete composite model" and is shown in Figure 17.

For the beams belonging to the mortar phase, the properties used in the previous examples (section 2) are used. For the aggregate phase, the elastic modulus and limit stress (σ_{lim}) are those of mortar multiplied by a factor of 2, and for the interface zone, the mortar properties are divided by a factor of 2. This choice of beam properties of the different phases illustrates a "strong aggregate – average mortar – weak interface" type of concrete.
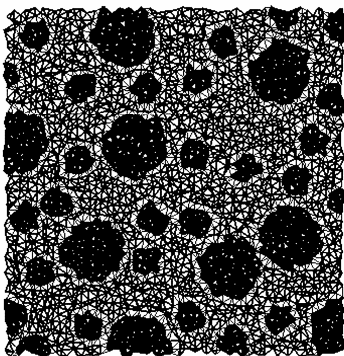
Figure 17 – Lattice model of the concrete composite. The linethickness of the beams is proportional to their limit stress (σ_{lim}).

Figure 18 shows that the resulting crack pattern is similar to the "homogenous" case of Figure 13. First left and right sides of the specimen will detach, followed by an extensive cracking at the centre of the model. The cracks tend now to follow the aggregate/mortar interfaces. Also, occasional aggregate cracking occurs, especially for larger aggregates near the corners or in the centre of the specimen. Comparing the stress-strain and stiffness-strain curves (figure 19) of concrete with the curves of plain mortar (figure 14), we observe that the initial stiffness drops from 25 to 18 GPa and that the stiffness decays faster due to the weak interface between mortar and aggregate. The maximum stress drops from 40 to 30 MPa attaining almost the same value of strain. After reaching peak stress, the stiffness decrease is more abrupt, so the concrete model behaves more brittle.
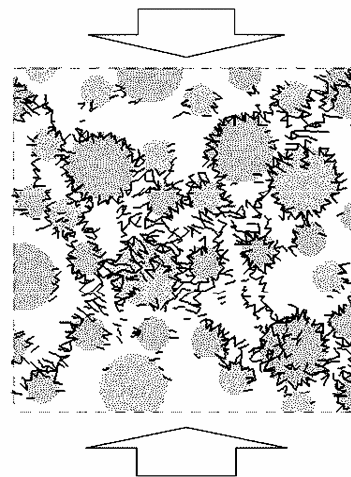
Figure 18 - Beams broken for a concrete composite model using an α = 0.5 (compressive strain = 3.0 mm/m).
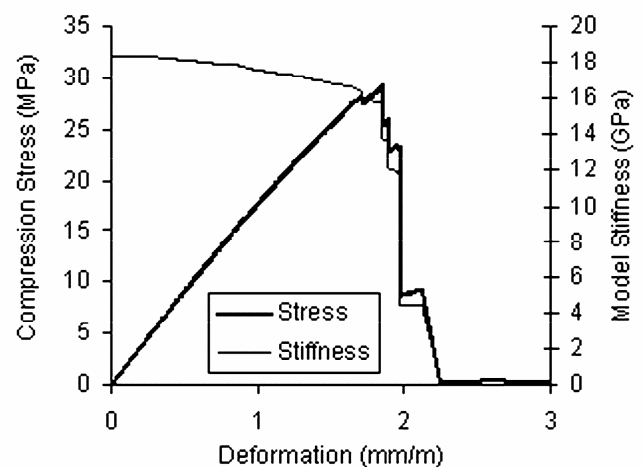
Figure 19 – Stress-strain and stiffness-strain curves for the concrete composite model with α = 0.5.

If the "unrestrained" boundary conditions are imposed, the crack pattern consists of oblique cracks following the 'weak' interfaces between mortar and aggregate (figure 20). Note that in this case of unrestrained boundary conditions the aggregates remain almost damage free. Comparing with the "homogenous" case (figure 15), the main cracks are now more vertical, which can be attributed to the presence of the aggregates, which seem to divert the cracks to an angle closer to the vertical. Figure 21 shows, as for the "homogenous" case, that the model behaves quite brittle. However, the change of the boundary conditions from restrained to unrestrained produces more noticeable differences on the initial stiffness and peak stress of the concrete model when compared with the homogeneous case. The initial stiffness increases from 18 to 21 GPa, and the peak stress decreases from 30 to 26 MPa.
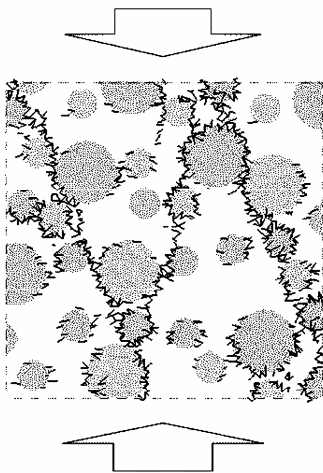
Figure 20 - Beams broken for a concrete composite "unrestrained" model using an α = 0.5 (compressive strain = 3.0 mm/m).
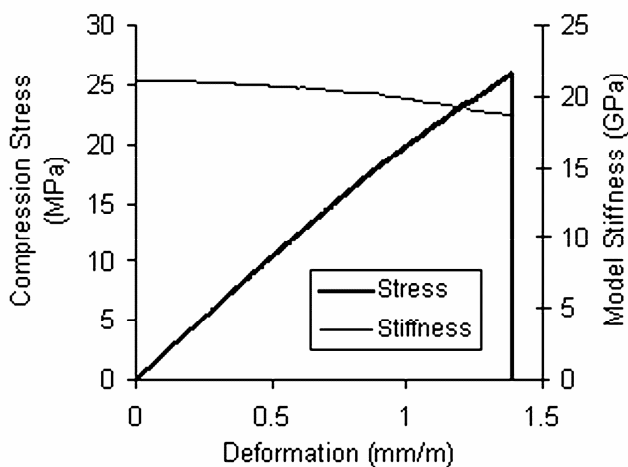
Figure 21 – Stress-strain and stiffness-strain curves for the concrete composite "unrestrained" model with α = 0.5.

6 CONCLUSIONS AND FUTURE DEVELOPMENTS

By the introduction of an extra step in the beams stiffness withdrawal, we have shown that the behaviour of the lattice model significantly improves for the simulation of cracking in compression. Although the number of calculations increases, the results presented in this paper are promising, as damage localisation is now likely to happen, giving realistic crack patterns.

For simulation of the tensile behaviour, the lattice model remains unchanged, because the two-step removal of the stiffness occurs for the same beam in two successive calculations. We conclude that the improvement of the model does not lead to fundamental changes to the lattice procedure, only some computational time is added. The simplicity of the lattice model is maintained, which is essential due to the large number of beam elements required.

Although the modified lattice model is able to retain some load transfer capacity and stiffness after reaching the peak stress the behaviour is still too brittle compared to the behaviour observed in real laboratory compression tests (Fig. 22). With the present formulation of the lattice model still more ductile behaviour is quite hard to attain. An alternative under investigation is the use of a 3D lattice with the modified lattice formulation.

The use of local softening on the elements has proven to be a valid way of obtaining a more ductile behaviour (Arslan et al. 2002, Bolander & Sukumar 2005) but the simplicity of the lattice model will be lost.
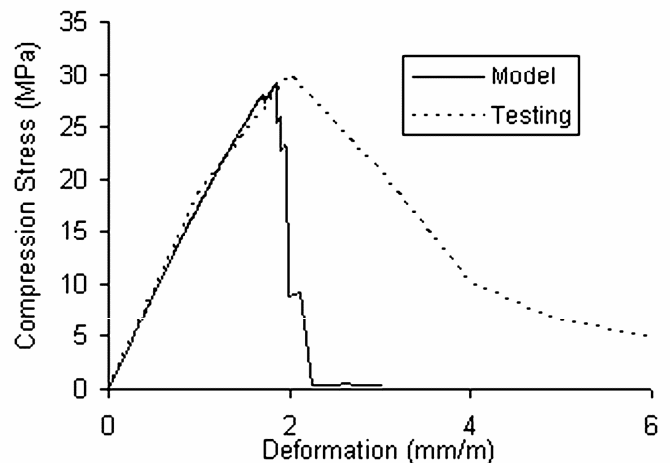
Figure 22 – Comparison between the laboratory test and the simulation with the modified lattice model.

REFERENCES

Schlangen, E. & Garboczi, E.J. 1996. "New method for simulating fracture using an elastically uniform random geometry lattice". In: Int. J. Engineering Sci. Vol 34, No 10, pp.1131-1144. Great Britain: Elsevier.

Schlangen, E. & Garboczi, E.J. 1997. "Fracture simulation of concrete using lattice models: Computational aspects". In: Engineering Fracture Mechanics Vol 57, No 2/3, pp.319-332. Great Britain: Elsevier.

Lilliu, G. & van Mier, J.G.M. 2000. "Simulation of 3D crack propagation with the lattice model". In: Proceedings Materials Week 2000. Available at 2005-07-08:
http://www.proceedings.materialsweek.org/proceed/mw2000_634.pdf

Arslan, A.; Ince, R. & Karihaloo, B. L. 2002. "Improved lattice model for concrete fracture", In Journal of Engineering Mechanics, Vol. 128, No 1, January 2002, pp. 57-65. USA: ASCE, ISSN 07333-93999/202/1-57-65.

Bolander, J.E. & Sukumar, N. 2005. "Irregular lattice model for quasistatic crack propagation", In: Physical Review B. 71 (9), Article 094106. USA: The American Physical Society.